

Polyurethane shape memory polymer: structure characterization and estimation of energy storage and dissipation during the tension process

Maria STASZCZAK¹ , Arkadiusz GRADYS² , Karol GOLASIŃSKI¹ , and Elżbieta Alicja PIECZYSKA¹ *

¹ Institute of Fundamental Technological Research, Polish Academy of Sciences, Pawińskiego 5B, 02-106 Warsaw, Poland

² Multidisciplinary Research Center, Cardinal Stefan Wyszyński University in Warsaw, Dewajtis 5, 01-815 Warsaw, Poland

Abstract. Shape memory polymers (SMP) are new multifunctional materials raising increasing interest in various functional applications. Among them, polyurethane shape memory polymers (PU-SMP) are particularly attractive due to their combination of shape memory, high strength and biocompatible properties. Developing new applications for PU-SMP requires comprehensive research on their characteristics. This work involved investigating the structure and mechanical behavior as well as characterizing the energy storage and dissipation of a thermoplastic PU-SMP with a glass transition temperature (T_g) of 25°C during tensile loading-unloading. The process of energy storage and dissipation in the PU-SMP was investigated based on the stress-strain curves recorded by a quasi-static testing machine and the temperature changes, accompanying the deformation process, obtained by using a fast and sensitive infrared camera. The results showed that the thermomechanical behavior of the examined PU-SMP depends significantly on the strain rate. At a higher strain rate, there are higher stress and related temperature changes, which lead to greater energy dissipation. However, the energy storage values estimated during the deformation process turned out to be not significant, indicating that the work supplied to the PU-SMP structure during loading is mainly converted into heat. It should also be noted that the structural investigation revealed no crystalline phase in the investigated PU-SMP.

Key words: shape memory polymer; infrared camera; thermomechanical couplings; energy storage and dissipation; tension test.

1. INTRODUCTION

Shape memory polymers (SMP) represent a group of stimuli-responsive materials that have the ability to fix a temporary deformed shape and then recover their original permanent shape under a suitable external stimulus [1–3] such as heat [4–7], light [8, 9], moisture [4, 10], magnetic field [11] or other triggers. The shape memory effect is a result of an adequate polymer molecular architecture, comprising two parts: the hard net points that build up the permanent shape of the SMP and the soft molecular switchable segments that are responsible for fixing its temporary shape [2, 3].

Thermo-responsive polyurethane shape memory polymers (PU-SMP) are an important class of new engineering smart materials among SMP. They exhibit good mechanical characteristics and demonstrate shape memory properties with a transition temperature that is generally the glass transition temperature (T_g) [1, 2, 12, 13]. PU-SMP are copolymers composed of discrete simple polymer segments (blocks) that are linked together in a chain [14]. They form a two-phase molecular structure: rigid amorphous domains (sometimes crystalline) that function as physical cross-links of the PU-SMP via van der Waals forces, ionic clusters or hydrogen bonding [15], and another amorphous softer phase [14]. T_g has a significant influence on the

functional behavior of PU-SMP, which is determined by the different molecular structures of the polymer segments above and below T_g [3, 12].

Figure 1 shows a schematic diagram of the shape memory effect in PU-SMP. After heating the material above T_g , the polymer softens and becomes rubbery, and due to this it can be processed and reshaped to a temporary shape easily. The temporary shape is fixed by cooling to a temperature below T_g followed by releasing the deformation (unloading). Reheating the polymer above T_g (under stress-free conditions) recovers the original shape thanks to the cross-links of the harder phase of the PU-SMP structure [3, 12, 16, 17].

PU-SMP are lightweight, biocompatible, relatively cheap and easy to process and recycle, and they possess high strain as well as shape recoverability under various conditions [2, 12]. Therefore, they show great potential to be used for new applications in various fields [12, 17, 18], particularly in the aerospace industry [5, 19, 20], robotics [21, 22], smart tex-

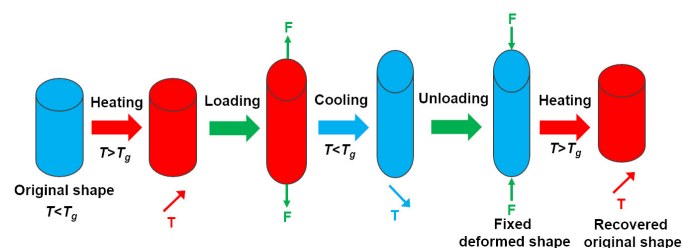


Fig. 1. Schematic diagram of the shape memory effect in SMP

*e-mail: epiecz@ippt.pan.pl

Manuscript submitted 2023-07-14, revised 2023-09-12, initially accepted for publication 2023-09-20, published in December 2023.

tiles [23–25], biomedical devices such as self-expandable vascular stents [26,27] and orthodontics [28,29] (Fig. 2). To ensure the reliable application of new, multifunctional materials, comprehensive research on their behavior under various conditions is necessary.

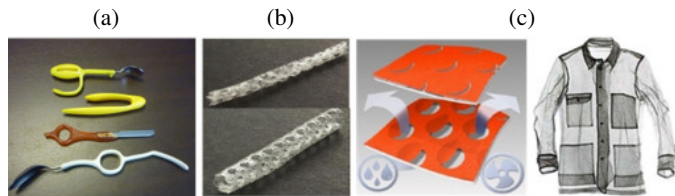


Fig. 2. Examples of PU-SMP applications: (a) tools for disabled people (SMP Technologies Inc.), (b) self-expandable vascular stents [26] and (c) smart textiles [23]

The loading and deformation process always modifies the energy state and in particular the temperature field of the strained material. Some of the external mechanical energy provided to the material in order to deform it is dissipated as heat, whereas the remainder contributes to the evolution of the material structure and after unloading it remains as stored energy E_s [30]. Knowledge of the transformation of mechanical work into heat, its dissipation and the stored energy process provides a better understanding of the mechanisms of material deformation under various conditions [31].

The stored energy demonstrates a change in the internal energy of the deformed materials and it has been a subject of theoretical study and experimental estimations. The first work concerning energy storage was published by Farren and Taylor in 1925 [32]. Next, in 1934, Taylor and Quinney introduced the concept of stored energy and showed that a large portion of the mechanical energy supplied to the metal sample is converted into heat, while the remaining portion is stored in its changed structure [30]. Bever et al. published an extensive review of early work within this field [31]. Chrysochoos and Martin proposed the thermodynamic background and experimental details of the unique method to investigate energy balance in metals subjected to deformation in a micro-calorimeter [33]. It was possible to identify particular components of the energy balance; however, the calibration of the calorimeter was complicated. Along with the development of new infrared techniques and advanced equipment, later studies have aimed at estimating the energy balance under room conditions, additionally using an infrared camera [34] and developing IRT [35–37].

The literature concerning estimation of stored energy in polymers is rather limited. Nevertheless, there are some examples of such works. Adams and Farris [38] conducted a study of the stored energy of polycarbonate during the deformation process carried out in an isothermal calorimeter, which allowed them to estimate the deformation work, heat and energy storage. They showed that the energy dissipated in the form of heat is about 50–80% of the deformation work, while the remaining part is stored in the material structure. Moreover, they found that if the process was carried out at 20°C, then the estimated amount of energy stored in this polymer depended on the ap-

plied strain rate: lower values were obtained for higher strain rates. Whereas, when the polymer was deformed at higher temperatures (20–65°C), the stored energy values did not depend significantly on the deformation temperature [38]. The authors also analyzed energy changes of other amorphous polymers during the uniaxial tension process. Those showed that the work used for the polymer deformation is not converted into heat, but rather stored in the polymer structure [39].

Research on the mechanical work expended on the deformation, dissipated heat and changes in internal energy carried out on amorphous polymers, i.e. polycarbonate, polystyrene and polyethylene-terephthalate, subjected to a compression process, was reported in [40]. The experimental method used in this work was that of deformation calorimetry. It was found that 45–85% of the mechanical work expended on the polymer deformation was stored in their structure.

More recently, Rittel [41] and Rittel and Rabin [42] published papers on energy dissipation, i.e. the heat generated by selected polymers during their cyclic loading. They presented both experimental and theoretical approaches, showing that the specific thermal response could be predicted, based on the general evolution of the dissipated energy throughout the experiment.

The energy-storage potential of self-healing shape memory polyimide was estimated by using dynamic mechanical analysis (DMA) during the shape memory process [43]. The authors found that upon triggering, this polymer can produce a stored energy of 0.105 J/g at an efficiency of 33.1%.

Heuwers et al. explored macroscopically the energy storage of shape memory natural rubber in the shape memory programming cycle [44]. They showed that the estimated energy stored in the rubber structure is highly dependent on the degree of cross-linking, as well as on the strain applied.

A method to estimate the local energy balance for polyamide 11 has been proposed in [45]. The authors used a comprehensive experimental approach, combining digital image correlation (DIC) and infrared thermography techniques (IRT). They tried to demonstrate how the heat sources are related to the internal energy dissipation mechanisms and the effects of thermo-mechanical couplings.

An increasing number of recently published papers have focused on the important issue of energy storage and dissipation in new advanced materials. However, to the best of our knowledge, the results of investigation of energy components in a polyurethane shape memory polymer have not been reported yet. Therefore, this paper concerns the estimation of the energy balance components and their evolution during the PU-SMP loading and deformation process, including structure characterization of this interesting shape memory polymer with a large application potential.

2. MATERIALS AND METHODS

2.1. Material

The research was performed on a thermoplastic PU-SMP denoted as MM2520, which is produced by SMP Technologies Inc. (Tokyo, Japan). Belt-type samples with the dimensions of

139 × 10 × 1.1 mm and a gauge length (GL) of 25 mm were used. The technical drawing of the sample designed for the tension test is shown in Fig. 3. Based on dynamic mechanical analysis in previous studies [46,47], T_g of the investigated PU-SMP is 25°C.

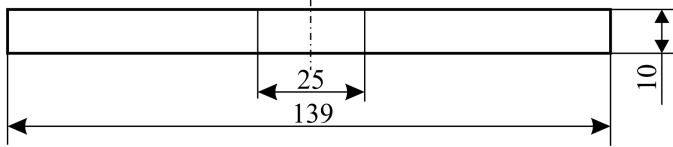


Fig. 3. Technical drawing of the PU-SMP sample

2.2. Structure characterization methods

In order to better understand the behavior of the material under various conditions, the structure of the analyzed PU-SMP was investigated. This investigation involved scanning electron microscopy (SEM), wide-angle X-ray scattering (WAXS) and specific heat measurement by means of differential scanning calorimetry (DSC).

The SEM investigation of the PU-SMP surface was conducted at room temperature using a JEOL JSM-6480 scanning electron microscope. To obtain better conductivity, the sample surface was covered with a thin carbon layer prior to observation.

WAXS investigation of the PU-SMP structure was conducted in transmission with a Bruker D8 Discover Diffractometer using Cu K α radiation and a wavelength of 1.5406 Å at 40 kV and 40 mA. The incident beam was formed using optics consisting of Göbel mirrors, a 0.3-mm circular slit and a 0.3-mm collimator. A Vantec-500 two-dimensional detector located 76.4 mm from the sample was used to record images. The detector-sample distance was calibrated using a silver behenate standard. All measurements were performed on stripe samples of 1 mm in thickness and 5 mm in width at room temperature, in both initial and deformed states, with uniaxial tensile loading on a laboratory drawing machine. The machine was mounted on the diffractometer stage in such a way that the incident beam was perpendicular to the sample surface transmitting through its middle part. Scattering of the incident beam by the sample was recorded using a 2D detector located behind the sample and positioned perpendicular to the incident beam.

Specific heat measurements were collected using a power-compensation Pyris 1 DSC (Perkin-Elmer) equipped with an Intracooler 2P cooling device. Temperature calibration was carried out using the melting points of indium and zinc. The calibration of the heat flow and of the specific heat capacity was performed using the melting heat of indium and specific heat of sapphire, respectively. The measurements were carried out on samples in the form of a disk with a thickness of ca. 1 mm and weighing ca. 30–40 mg, in the temperature range of –5 to 55°C, under high purity nitrogen (99.999%) flow at 20 ml/h. The experiments were performed by using the StepScan method in a stepwise heating mode with a temperature increase of 1°C at a rate of 75°C/min, followed by an isothermal step of approximately 2 min to achieve an equilibrium state of the heat flow. As

a result, the sample was subjected to the action of non-periodic heat pulses. Analysis of the measured heat flow as a function of time, using the Laplace transform, led to the determination of the heat capacity spectrum, allowing, in effect, for determination of precise heat capacity. The theoretical basis and detailed description of the method are presented in [48,49].

2.3. Experimental details for PU-SMP tensile loading and the related temperature changes

The tension tests were performed on an MTS 858 testing machine at room temperature with two strain rates, namely $2 \cdot 10^{-1} \text{ s}^{-1}$ and $2 \cdot 10^0 \text{ s}^{-1}$. In each test, the strain rate was the same during loading and unloading. The stress and strain quantities presented in the diagrams were related to the current (instantaneous) values of the sample cross-section, obtaining the so-called “true stress” and “true strain” values, and were calculated, according to Eq. (1) and Eq. (2), respectively [50]:

$$\sigma = \frac{F \cdot (l_0 + \Delta l)}{l_0 \cdot S_0}, \quad (1)$$

$$\varepsilon = \ln \left(\frac{l_0 + \Delta l}{l_0} \right), \quad (2)$$

where: Δl is the change in specimen gauge length determined on the basis of the extensometer, l_0 is the initial gauge length (GL), F is the instantaneous force value, and S_0 is the initial cross-section.

The fast and sensitive ThermoCam™ Phoenix infrared IR camera was used to determine the temperature changes of the analyzed PU-SMP during the tension process in a contactless manner. The IR camera parameters were as follows: wavelength range of 3–5 μm , maximum frequency of 538 Hz, window size of 160 × 256 pixels and thermal sensitivity of up to 0.02°C. The IR camera records the infrared radiation emitted by the specimen, which allows for identifying temperature distributions of the specimen surface during the deformation process, i.e. thermograms. Based on the temperature distributions obtained, the mean temperatures were determined considering the coefficient of emissivity of 0.96 and the internal gauge area of the PU-SMP sample of 25 × 10 mm, avoiding boundary effects. The temperature change ΔT denotes the difference between the mean value of the temperature calculated for the gauge area of the tested specimen at each instant of straining $T(t)$ and the mean temperature of the same area before the deformation $T(t_0)$ (Eq. (3)):

$$\Delta T = T(t) - T(t_0). \quad (3)$$

2.4. Energy balance methodology

The energy phenomenon accompanying elastoplastic deformation is closely connected to complex thermomechanical couplings, i.e. interactions between mechanical and thermal effects, and can be studied at different levels of the scale [33–35]. In this paper, we focus on the macroscopic scale approach to this research problem.

The energy balance of PU-SMP was estimated based on the mechanical characteristics that were obtained: (i) during loading at room temperature; (ii) with two appropriately high strain

rates of $2 \cdot 10^{-1} \text{ s}^{-1}$ and $2 \cdot 10^0 \text{ s}^{-1}$, for which the process conditions are considered adiabatic; and (iii) for two strain ranges $\varepsilon = 0.6$ and $\varepsilon = 1.18$, where the deformation was macroscopically homogeneous.

Figure 4 shows a schematic representation of the methodology used in this approach to determine inelastic mechanical energy W_{in} expended on plastic deformation during uniaxial tension based on the force versus displacement curve. In the case of elastic-plastic solids, i.e. metals and alloys, W_e is the work expended on elastic deformation, while W_{in} denotes the work of plastic deformation W_p . Upon loading, initially the elastoplastic material deforms elastically (0-A). Then, after exceeding the yield limit, it begins to deform plastically. As a result, the load-displacement relationship becomes non-linear (A-B). Then, during unloading (section B-C), this relationship is usually again linear and parallel to the elastic part of the loading curve (0-A). Therefore, the work of plastic deformation W_p can be determined for any point of the deformation process, without sample unloading, taking into account the mass of the working part of the sample m and assuming that the elastic properties of the material in the considered range do not depend on changes in its microstructure [51, 52].

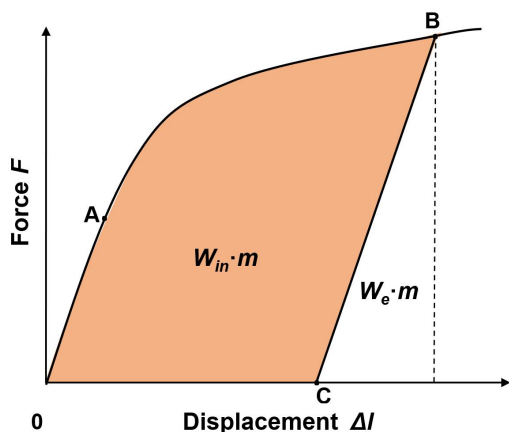


Fig. 4. Scheme of the method to determine the work expended on inelastic deformation during tension loading based on the force vs. displacement curve

Analysis of the energy balance of SMP is more complex because it includes the energy component expended for the shape memory effect, while inelastic energy W_{in} is defined as the work expended on irreversible deformation associated with polymer structure changes. Moreover, the unloading curve is not linear and not parallel to the initial stage of the loading curve. Nevertheless, this approach can be also used for polymers by considering other material parameters [53], as explained in Section 3.3.

3. RESULTS AND DISCUSSION

3.1. PU-SMP structure characterization

The SEM images obtained at $500\times$ and $2500\times$ magnification are shown in Fig. 5a and 5b, respectively. The surface of the PU-SMP reveals the influence of the block copolymer bulk mor-

phology. At $500\times$ magnification (Fig. 5a), the longitudinal strip organization is visible, which can be attributed to interactions between adjacent domains or forced chain orientation during the material production. The microphase separation for the examined PU-SMP sample is also evident. It can be supposed that the continuous phase is formed by the amorphous soft phase domains. At $500\times$ magnification, the dispersion of some irregularly shaped inclusions of the second hard phase as lighter areas in a continuous phase can be observed, which becomes more pronounced at $2500\times$ magnification (Fig. 5b). The phase separation in the analyzed PU-SMP sample takes place as a result of limited compatibility between hard and soft segments [54].

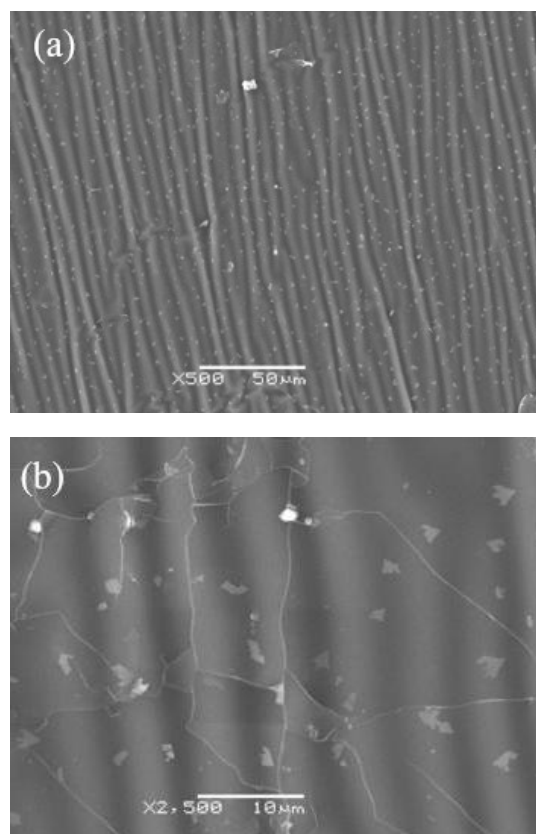


Fig. 5. SEM images of the examined PU-SMP sample at: (a) $500\times$ and (b) $2500\times$ magnification

WAXS was conducted on the samples in the initial state (without deformation) as well as on the samples subjected to uniaxial tensile loading in a stepwise loading mode and a continuous mode without pausing. X-ray scattering images in the stepwise loading mode were recorded at each step of the steady strain state: undeformed sample ($\varepsilon = 0\%$) and at subsequent stages of step tensile loading to strain values of 70%, 110% and 125%. The loading led to a sample rupture at a strain value of $\approx 133\%$. For the sample subjected to continuous loading, the WAXS image was recorded at a strain value of 143%.

Characterization of orientation with respect to the loading direction was performed by a commonly used procedure relying on the analysis of the distribution of intensity over the azimuthal angle ϕ . The plots covering the ϕ range from 0° to

90° are presented in Fig. 6. Minimum intensity is at $\phi = 0^\circ$, corresponding to the loading direction, and maximum intensity is at $\phi = 90^\circ$, corresponding to the direction perpendicular to the loading direction. Figure 6 also shows that the minimum value of intensity at $\phi = 0^\circ$ decreases as the strain increases. This phenomenon can be attributed to the change in the orientation of macromolecules with strain. Interestingly, for the sample under no strain, the intensity distribution over ϕ is not constant, as it would be if there was a lack of orientation, but it shows a similar intensity distribution with a smaller change in intensity with ϕ . This finding may suggest the existence of some initial orientation along the drawing direction.

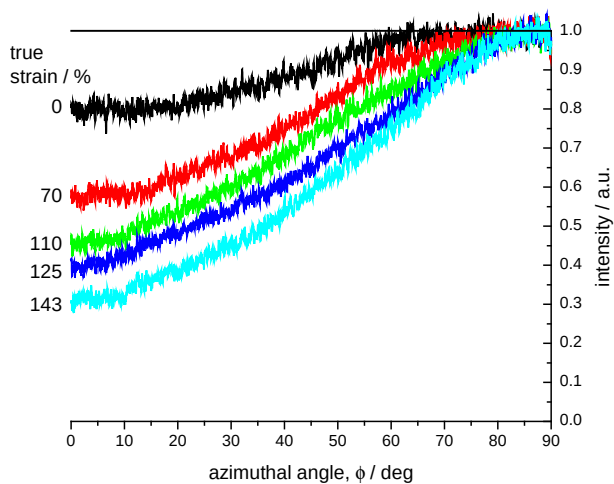


Fig. 6. Azimuthal distribution of intensity determined for the analyzed PU-SMP samples at different strain values

Based on the WAXS results, the analyzed PU-SMP is in an amorphous state, indicated by the presence of a single broad symmetrical amorphous “halo” with a maximum at the scattering angle 2θ of 22° (Fig. 7) and a lack of diffraction peaks. The position of the amorphous halo is similar to the halo found in other amorphous polyurethane systems [55]. In addition, uniaxial deformation does not induce crystallization because there are no diffraction peaks.

The intensity profiles over the diffraction angle 2θ along the loading direction show evidence of the additional weak structural feature as a small peak, indicated by an arrow at $2\theta = 11^\circ$ (Fig. 7a). On the other hand, this weak peak is not visible on intensity profiles over 2θ along the perpendicular direction (Fig. 7b). This peak indicates the presence of a very small fraction ($< 0.1\%$) of a phase characterized by very low structural symmetry showing periodicity in only one direction (001).

The WAXS images were also used for quantitative characterization of the structure orientation of the investigated samples by the commonly used Herman orientation factor f_a [56]. For the investigated PU-SMP, f_a takes negative values starting from -0.03 at 0 strain and decreases as the strain increases to -0.13 at a strain of 143%. The d-spacing values related to average intermolecular distances were determined from the 2θ position of the respective scattering peak. In the case of the amorphous phase, the intermolecular distance d , equal to 4.07 \AA , is a typi-

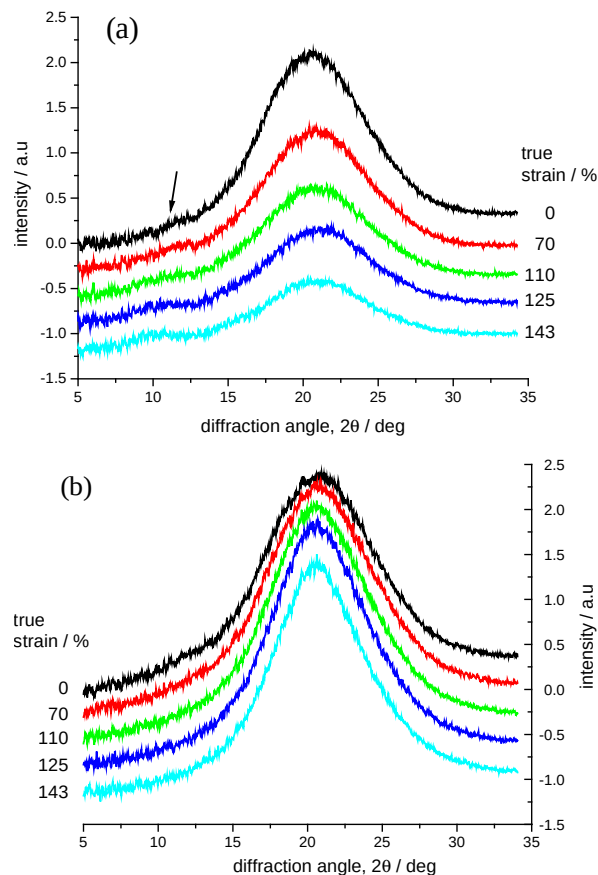


Fig. 7. Intensity profiles along (a) the loading direction, $\phi = 0^\circ$ and (b) the perpendicular direction, $\phi = 90^\circ$, determined from WAXS images for samples at various strain values. Intensity is integrated over $\phi - 15^\circ / \phi + 15^\circ$ range; the arrow shows a small peak attributed to the phase of low structural symmetry

cal value for polymer systems. The observed decrease in intermolecular distance is expected as a natural consequence accompanying the orientation of molecules under increasing strain. The small peak associated with the low-symmetry phase is characterized by an increase in d-spacing with deformation: as strain increases, this phase becomes more oriented and strained, and it leads to an increase in distance d above the initial value (7.7 \AA) to 8.5 \AA at a strain value of 143%.

Precise specific heat capacity data were obtained using DSC and the special analysis method described in [48, 49]. The specific heat capacity versus temperature curve is presented in Fig. 8. The data were obtained for the first time for this type of polymer (PU-SMP) and are presented as an average from three measurements.

As can be seen from the graph, the standard deviations are very small, indicating high precision of the method. Below 20°C , specific heat capacity increases abruptly, indicating the glass transition range. T_g is estimated as ca. 7°C . Above 20°C , a further increase in c_p becomes a low linear function of temperature. The determined values of the specific heat capacity of the investigated PU-SMP are between 1.35 and $1.9 \text{ J/(g}\cdot\text{K)}$. At room temperature, the specific heat capacity is around $1.80 \text{ J/(g}\cdot\text{K)}$.

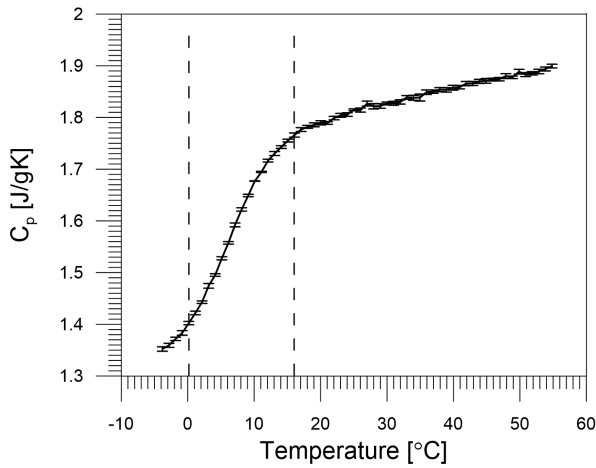


Fig. 8. Average specific heat c_p vs. temperature curve with standard deviations

In summary, because T_g of the investigated PU-SMP as determined by DMA is 25°C, the T_g at 7°C which is determined as c_p increase by DSC (Fig. 8), is probably related only to the soft phase. On the other hand, the presence of the hard phase is probably indicated by the WAXS low symmetry peak located at $2\theta = 11^\circ$ (Fig. 7a). However, these issues require further investigation.

3.2. PU-SMP tensile loading and the related temperature changes

The PU-SMP samples with T_g of 25°C were subjected to tensile loading-unloading at two strain rates: $2 \cdot 10^{-1} \text{ s}^{-1}$ and $2 \cdot 10^0 \text{ s}^{-1}$ in the direction in line with the longitudinal strip organization shown in Fig. 5a.

The obtained force F versus the crosshead displacement Δl curves in the strain range of up to 0.6 and 1.18 are presented in Fig. 9a and 9b, respectively. For the higher strain rate, there are significantly higher force values in both ranges of deformation. However, the displacement values after unloading do not change significantly for the same deformation range. For the test conducted within the strain range of 0.6, it equals 6.4 mm at higher strain rate, while at lower strain rate it equals 7.3 mm; for the test conducted within the strain range of 1.18, it is 12.9 mm at higher strain rate, while at lower strain rate it is 14.9 mm.

Figure 10 presents the stress σ and temperature change ΔT versus strain ε curves developed for the PU-SMP samples. In the initial stage of deformation, for both strain ranges and strain rates, there is a slight drop in sample temperature, called a thermoelastic effect, that accompanies the elastic loading and unloading of any solids [57]. This phenomenon has also been demonstrated by authors for PU-SMP in previous studies [46, 58–60]. Subsequently, as the strain increases, both the stress values and the sample temperature increase (Fig. 10a and 10b).

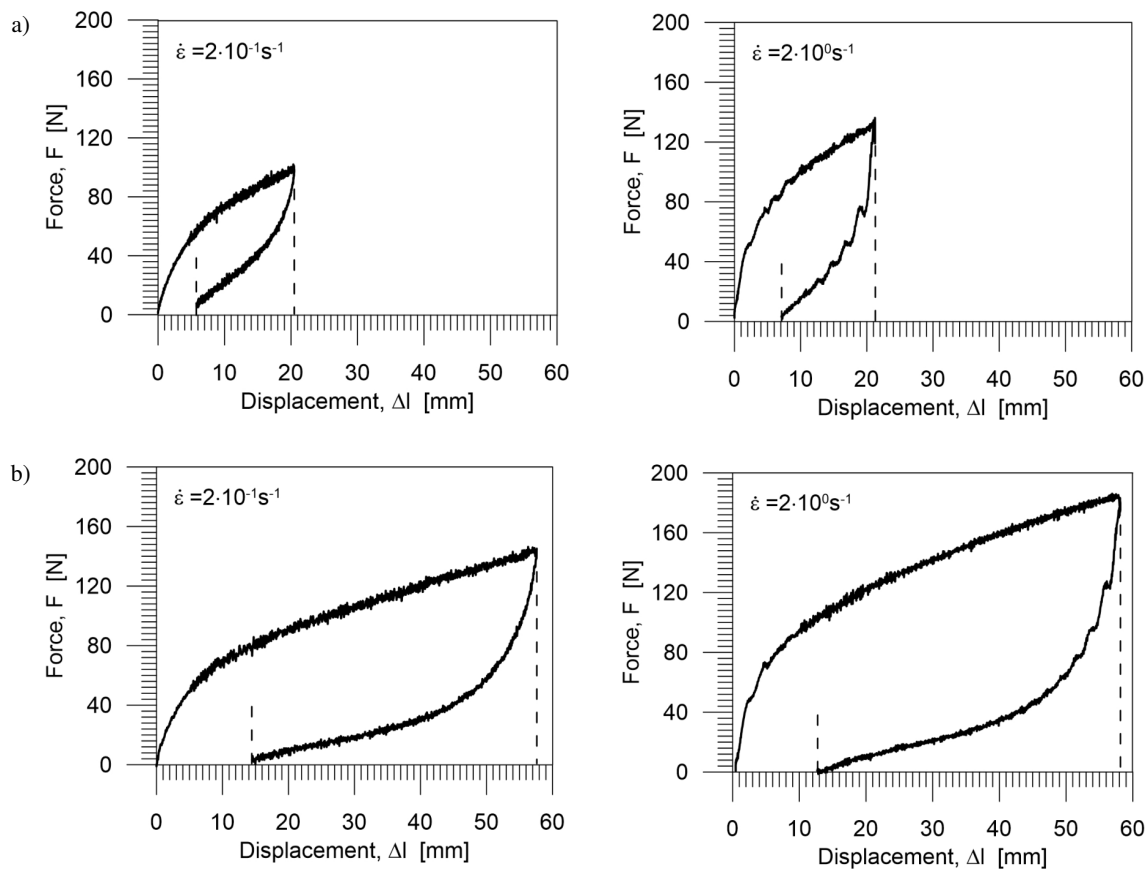


Fig. 9. Force F vs. displacement Δl obtained during tension of the investigated PU-SMP samples at the strain rate of $2 \cdot 10^{-1} \text{ s}^{-1}$ (left) and $2 \cdot 10^0 \text{ s}^{-1}$ (right) in the strain range of (a) 0.6 and (b) 1.18

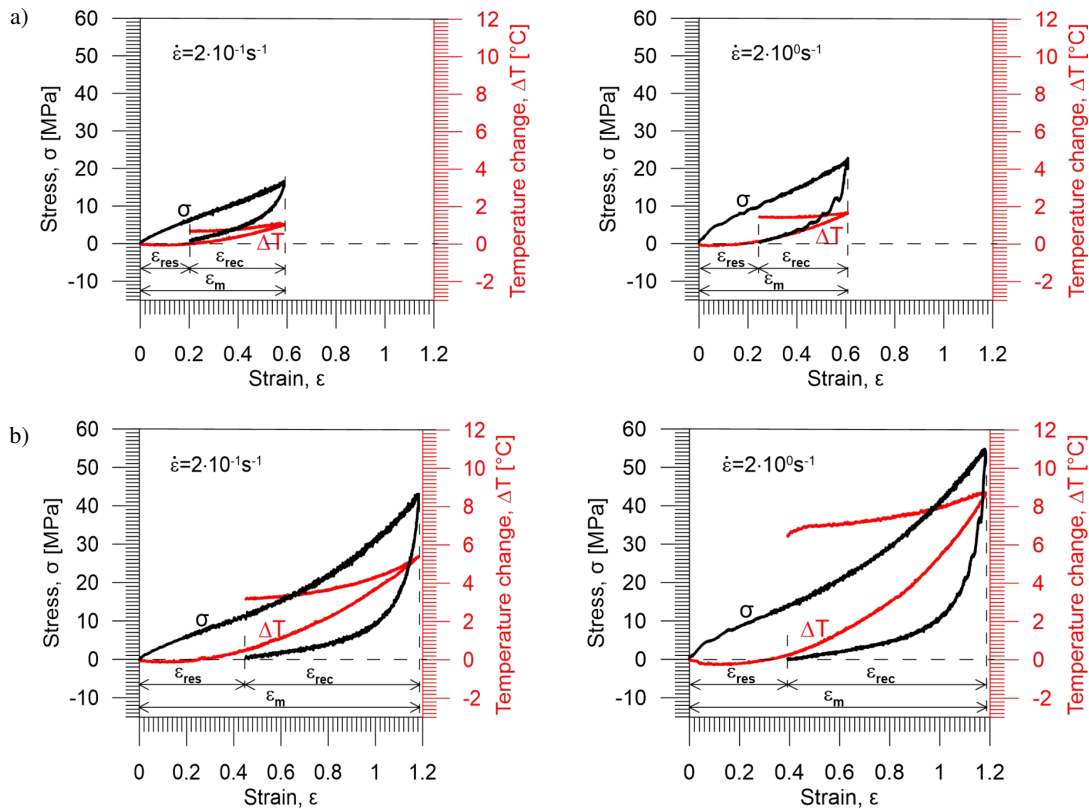


Fig. 10. Stress σ and temperature change ΔT vs. strain ϵ during PU-SMP tension at the strain rate of $2 \cdot 10^{-1} \text{ s}^{-1}$ (left) and $2 \cdot 10^0 \text{ s}^{-1}$ (right) in the strain range of (a) 0.6 and (b) 1.18

The results show that the higher the strain rate, the higher the stress and temperature changes of the PU-SMP samples. For a higher strain rate, the deformation processes occur more dynamically and the test conditions are closer to adiabatic. This outcome demonstrates strong thermomechanical couplings in the shape memory polymer.

The maximum strain to which the sample was loaded ϵ_m , the strain recovered during unloading ϵ_{rec} and the residual strain ϵ_{res} are marked in Fig. 10 and presented in Table 1. Moreover, the $\epsilon_{res}/\epsilon_{rec}$ and $\epsilon_{rec}/\epsilon_m$ ratios were calculated (Table 1). The lower the $\epsilon_{res}/\epsilon_{rec}$ ratio and the higher the $\epsilon_{rec}/\epsilon_m$ ratio, the greater the shape recovery to the original shape that is obtained. The highest parameter values occur for loading at a strain range of 1.18 with the strain rate of $2 \cdot 10^0 \text{ s}^{-1}$. During the unloading, which takes place at a temperature of slightly below T_g , some strain recovery is observed. The strain recovery is a result of the

Table 1

Maximum strain ϵ_m , recovered strain ϵ_{rec} and residual strain ϵ_{res} after unloading and the calculated ratios of these parameters

| Strain rate | ϵ_m | ϵ_{res} | ϵ_{rec} | $\epsilon_{res}/\epsilon_{rec}$ | $\epsilon_{rec}/\epsilon_m$ |
|----------------------------------|--------------|------------------|------------------|---------------------------------|-----------------------------|
| $2 \cdot 10^{-1} \text{ s}^{-1}$ | 1.18 | 0.45 | 0.73 | 0.61 | 0.62 |
| $2 \cdot 10^0 \text{ s}^{-1}$ | 1.18 | 0.39 | 0.79 | 0.50 | 0.67 |
| $2 \cdot 10^{-1} \text{ s}^{-1}$ | 0.6 | 0.25 | 0.34 | 0.75 | 0.57 |
| $2 \cdot 10^0 \text{ s}^{-1}$ | 0.6 | 0.30 | 0.31 | 0.95 | 0.51 |

PU-SMP structure and the ability of hard segments to retain the original shape. On the other hand, ϵ_{res} remains quite large after unloading because the soft segments of the PU-SMP structure are frozen at low temperature.

The maximum temperature change ΔT_{max} , the maximum stress value $\Delta\sigma$ (for the maximum strain value) and the initial sample temperature T_0 needed for the PU-SMP energy estimation were also determined during the tensile test and are presented in Table 2.

Table 2

Determined parameters used in energy estimation of the PU-SMP with $T_g = 25^\circ\text{C}$

| Parameter used in energy estimation | Strain $\epsilon = 0.6$ | | Strain $\epsilon = 1.18$ | |
|-------------------------------------------------|----------------------------------|-------------------------------|----------------------------------|-------------------------------|
| | $2 \cdot 10^{-1} \text{ s}^{-1}$ | $2 \cdot 10^0 \text{ s}^{-1}$ | $2 \cdot 10^{-1} \text{ s}^{-1}$ | $2 \cdot 10^0 \text{ s}^{-1}$ |
| Maximum temperature change ΔT_{max} [K] | 1.03804 | 1.63680 | 5.39656 | 8.70637 |
| Maximum stress $\Delta\sigma$ [MPa] | 14.64568 | 21.42659 | 43.04629 | 52.71138 |
| Initial sample temperature T_0 [K] | 295.45 | 295.35 | 294.35 | 294.15 |

3.3. Investigation of the energy balance components in the PU-SMP subjected to tension

The methodology used for energy estimation during the loading process of the PU-SMP with $T_g = 25^\circ\text{C}$ is discussed based on the mechanical characteristics obtained for the polymer, as mentioned in Section 2.3, and is presented in Fig. 11.

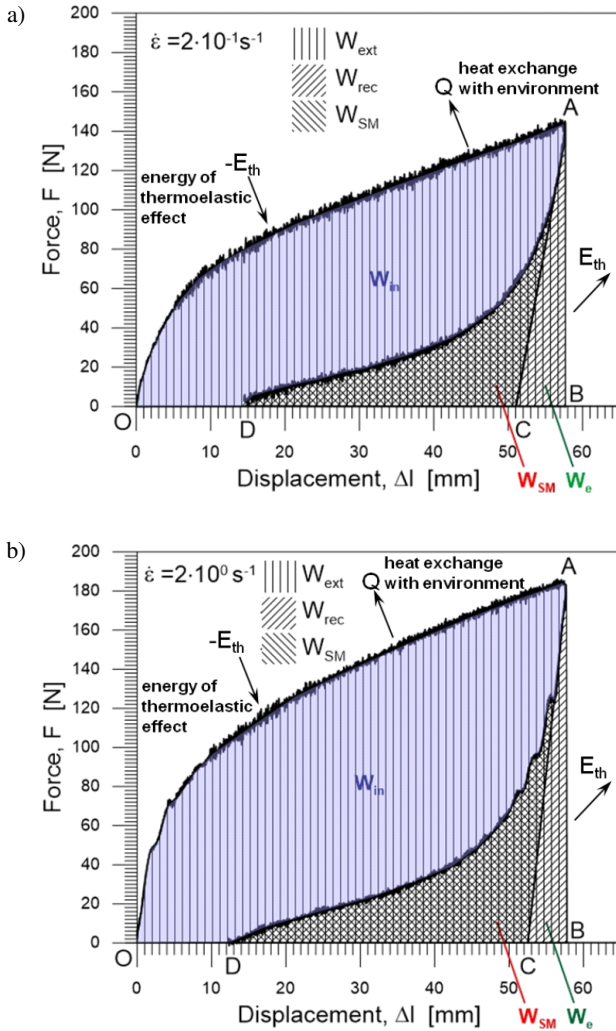


Fig. 11. Scheme of energy estimation during the PU-SMP loading-unloading cycle at a strain rate of (a) $2 \cdot 10^{-1} \text{ s}^{-1}$ and (b) $2 \cdot 10^0 \text{ s}^{-1}$

Force F versus displacement Δl curves for strain rates of $2 \cdot 10^{-1} \text{ s}^{-1}$ and $2 \cdot 10^0 \text{ s}^{-1}$ are shown in Fig. 11a and 11b, respectively. The arrows indicate specific components of the energy balance of the sample, i.e. the heat exchange with the environment Q and the energy of the thermoelastic effect E_{th} .

The total external mechanical energy W_{ext} delivered to the gauge part of the sample from the beginning of the deformation process to the point marked by B is equal to the area under the OAB curve. It can be decomposed into recoverable energy W_{rec} (DAB area) and inelastic energy W_{in} (OAD area). Then, W_{ext} can be defined based on Eq. (4):

$$W_{ext} = W_{rec} + W_{in}. \quad (4)$$

As it was mentioned earlier, in the case of polymers W_{in} denotes the work expended on irreversible deformation. The work consumed for the elastic deformation equals the area under the CAB curve and is designated W_e [51, 52]. However, in the case of shape memory polymers, the work used for reversible deformation W_{rec} can be divided into the work expended on the reversible elastic deformation W_e and additional work used for the shape memory effect W_{SM} (Eq. (5)):

$$W_{rec} = W_e + W_{SM}. \quad (5)$$

If the reversible part of the energy is subtracted from the total work expended on the sample deformation, then the work used for irreversible deformation is W_{in} . In Fig. 11 it is denoted by the OAD area, which includes energy dissipated as heat in the loading process W_d and energy stored in the material E_s (Eq. (6)):

$$W_{in} = W_d + E_s. \quad (6)$$

The entire dissipated energy in the process of deformation W_d that denotes the heat transferred to the environment by the gauge length of the sample during the deformation process Q should also consider thermal losses during the deformation process, resulting from thermal conductivity W_{ind} , convection W_{conv} and radiation W_{rad} , as shown in Eq. (7):

$$W_d = Q + W_{ind} + W_{conv} + W_{rad}. \quad (7)$$

In this analysis, the heat loss resulting from the conductivity to the grips of the testing machine can be neglected, because they are not as significant for polymers as they are for metals. The heat losses related to convection and radiation were also negligible, especially because the analyzed deformation process was carried out at a relatively high strain rate, i.e. under conditions close to adiabatic. With this simplification, the energy dissipated as heat W_d is equal to Q , and its value is calculated by multiplying the specific heat of the material c_p and the sample temperature change caused by the deformation ΔT based on Eq. (8):

$$W_d = Q = c_p \cdot \Delta T, \quad (8)$$

where: c_p is the specific heat of the PU-SMP and ΔT is the sample temperature change determined in a contactless manner using an infrared camera.

Assuming that the process is adiabatic, the energy balance includes an additional component – the energy of the thermoelastic effect E_{th} equal to the energy associated with the temperature drop. It is calculated with Eq. (9):

$$E_{th} = -\frac{\alpha T_0 \Delta \sigma}{\rho}, \quad (9)$$

where: α is the thermal expansion coefficient, T_0 is the sample temperature on an absolute scale, $\Delta \sigma$ is the stress change and ρ is the PU-SMP sample density.

Thus, the work expended on irreversible deformation can be expressed with Eq. (10):

$$W_{in} = E_s + Q - E_{th}. \quad (10)$$

From Eq. (4), (5) and (10), it follows that the total external mechanical energy expended on deformation is equal to (Eq. (11)):

$$W_{\text{ext}} = E_s + Q - E_{\text{th}} + W_e + W_{\text{SM}}. \quad (11)$$

The energy stored during the deformation process equals (Eq. (12)):

$$E_s = W_{\text{ext}} - W_{\text{rec}} + E_{\text{th}} - Q. \quad (12)$$

The particular energy values were determined per unit of the mass of the sample gauge length GL.

The material parameters of the investigated PU-SMP used to estimate energy balance during the tension process are shown in Table 3. The value of the specific heat c_p was presented with calorimeter tests, as discussed in Section 3.1. The value of the thermal expansion coefficient α was taken from the literature for similar materials [61]. The density of PU-SMP was measured using Archimedes' principle; it equals 1.35 g/cm^3 .

Table 3

Material parameters used for energy estimation of the PU-SMP with $T_g = 25^\circ\text{C}$

| Material parameter | Value |
|----------------------------------------------------------|---------------------------|
| Density ρ_0 , [g/cm ³] | 1.35 |
| Specific heat c_p ($T = 23^\circ\text{C}$) [J/(g·K)] | 1.80 |
| Specific heat c_p ($T = 32^\circ\text{C}$) [J/(g·K)] | 1.82 |
| Coefficient of thermal expansion α [1/K] | $1.48 \cdot 10^{-4}$ [61] |

Energy components for the PU-SMP with $T_g = 25^\circ\text{C}$ were estimated using Eq. (2) and (6)–(10). The obtained values of particular energies calculated using the energy balance equation, namely the energy of total work W_{ext} , the work expended on reversible deformation W_{rec} and irreversible deformation W_{in} , the dissipated heat Q , the energy of the thermoelastic effect E_{th} and the energy stored in the material E_s are presented in Table 4. In addition, the calculated $W_{\text{rec}}/W_{\text{in}}$ and $W_{\text{in}}/W_{\text{ext}}$ ratios at strain ranges of 0.6 and 1.18 are included in Table 4.

A comparison of the estimated energies for the PU-SMP during the tension loading-unloading process at strain rates of $2 \cdot 10^{-1} \text{ s}^{-1}$ and $2 \cdot 10^0 \text{ s}^{-1}$ is demonstrated in Fig. 12a and 12b, respectively.

It can be noticed that the total work W_{ext} , the work expended on irreversible deformation W_{in} as well as dissipated heat Q depend on the strain rate. At the higher strain rate, these values are higher. On the other hand, the work expended on reversible deformation W_{rec} is similar for both strain rates and thus does not depend on the strain rate. Here we observe a certain analogy to the behavior of TiNi shape memory alloys [62]. The dissipated heat Q is greater for the higher strain rate, while the differences in the values of the energy of the thermoelastic effect E_{th} are not very notable.

According to the results obtained, the estimated stored energy E_s at the strain rate of $2 \cdot 10^{-1} \text{ s}^{-1}$ is 0.0144 J/g for the strain range of 0.6, while the estimated stored energy for

Table 4

Estimated energy values for the PU-SMP with $T_g = 25^\circ\text{C}$ within the strain range of 0.6 and 1.18

| Estimated value | Strain $\varepsilon = 0.6$ | | Strain $\varepsilon = 1.18$ | |
|--------------------------------|----------------------------------|-------------------------------|----------------------------------|-------------------------------|
| | $2 \cdot 10^{-1} \text{ s}^{-1}$ | $2 \cdot 10^0 \text{ s}^{-1}$ | $2 \cdot 10^{-1} \text{ s}^{-1}$ | $2 \cdot 10^0 \text{ s}^{-1}$ |
| W_{ext} [J/g] | 3.7959 | 5.5867 | 16.8746 | 22.7347 |
| W_{rec} [J/g] | 1.573499 | 1.5927 | 4.4091 | 5.2763 |
| W_{in} [J/g] | 2.2224 | 3.9940 | 12.4654 | 17.4584 |
| Q [J/g] | 1.8919 | 2.9832 | 9.7130 | 15.6701 |
| E_{th} [J/g] | -0.8109 | -1.1860 | -2.3746 | -2.9058 |
| E_s [J/g] | 0.0144 | 0.3170 | 1.3634 | 0.0885 |
| $W_{\text{rec}}/W_{\text{in}}$ | 0.7102 | 0.3938 | 0.3537 | 0.3018 |
| $W_{\text{in}}/W_{\text{ext}}$ | 0.5855 | 0.7149 | 0.7387 | 0.7679 |

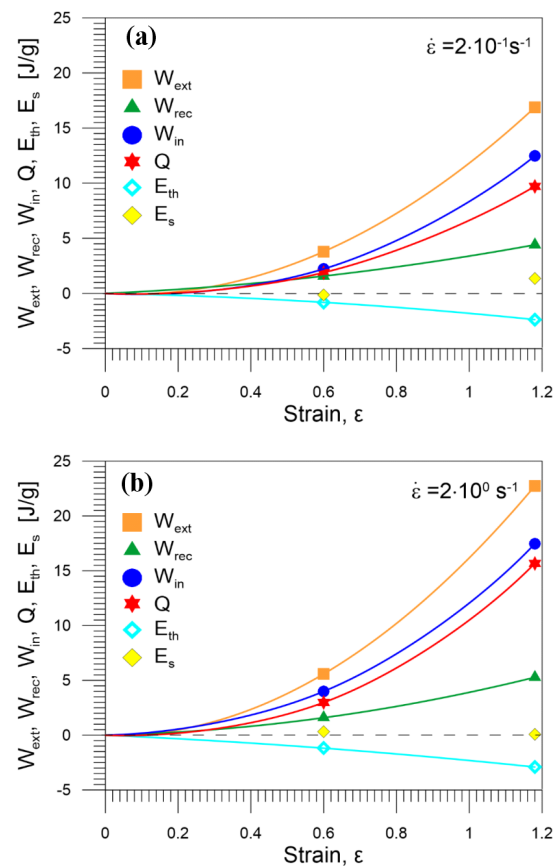


Fig. 12. Comparison of estimated W_{ext} , W_{rec} , W_{in} , Q , E_{th} and E_s vs. strain ε for the strain rate of (a) $2 \cdot 10^{-1} \text{ s}^{-1}$ and (b) $2 \cdot 10^0 \text{ s}^{-1}$

the strain range of 1.18 is 1.3634 J/g . On the other hand, at the strain rate of $2 \cdot 10^0 \text{ s}^{-1}$ and for the strain range of 0.6, E_s is 0.3170 J/g , while for the strain range of 1.18, E_s is 0.0885 J/g (Fig. 12). Therefore, based on the macroscopic scale energy analysis, it was found that in the selected deformation range, considered to be macroscopically homogeneous, a small amount of energy supplied to the PU-SMP is stored in its structure. This means that the energy is mostly dissipated as heat.

Another hypothesis may be that the energy is compensated between the hard and soft segments in shape memory polymer structure, which is planned to be checked on another type of a shape memory polymer.

4. CONCLUSIONS

A multifunctional smart polyurethane shape memory polymer with $T_g = 25^\circ\text{C}$, characterized by unique properties and large application potential, was subjected to structure characterization, mechanical testing and thermomechanical analysis. The results have demonstrated its good mechanical and shape memory properties and high sensitivity to the strain rate with respect to the mechanical curves, their related temperature changes and the energy balance component values. Structural analysis did not show a crystalline phase in the PU-SMP in the examined strain range.

Experimental estimation of the macroscopic scale energy balance in the PU-SMP was conducted for the tension loading process at two strain rates under room conditions. The particular components of the energy balance were determined and discussed. The mechanical energy W_{ext} provided to the PU-SMP sample during its deformation process, the inelastic energy W_{in} and the dissipated energy depend on the strain rate applied. The higher the strain rate, the higher the energy values that were obtained. However, the recoverable energy W_{rec} and the energy of thermoelastic effect E_{th} almost do not depend on the strain rate. The investigated PU-SMP exhibits a certain similarity to the behavior observed in previous research on TiNi shape memory alloys.

The estimated values of the stored energy E_s for both strain rates and strain ranges turned out to be insignificant. This finding means that only a small amount of energy is stored in the PU-SMP structure during the deformation process. Therefore, it can be concluded that the energy is mostly dissipated, i.e. converted into heat. These properties can be desirable in some specific applications in which large heat dissipation is important.

ACKNOWLEDGEMENTS

This research was funded by the National Science Centre (NCN) Poland: grant numbers 2011/01/M/ST8/07754 (Harmonia – a collaboration between the Institute of Fundamental Technological Research of the Polish Academy of Sciences (IPPT PAN) and the Aichi Institute of Technology AIT, Japan) and 2017/27/B/ST8/03074. The authors are grateful to R. Matsui and K. Takeda for highly useful advice; to M. Cristea for obtaining the DMA data; to S. Golba for performing scanning electron microscopy; and to S. Hayashi, SMP Technologies Inc., Tokyo, Japan, for providing the PU-SMP material.

REFERENCES

- [1] S. Hayashi, "Properties and applications of polyurethane-series shape memory polymer," *Int. Prog. Urethanes*, vol. 6, pp. 90–115, 1993.
- [2] S. Hayashi, S. Kondo, P. Kapadia, and E. Ushioda, "Room-temperature-functional shape-memory polymers," *Plast. Eng.*, vol. 51, pp. 29–31, 1995.
- [3] A. Lendlein and S. Kelch, "Shape-Memory Polymers," *Angew. Chem. Int. Ed.*, vol. 41, no. 12, pp. 2034–2057, 2002, doi: [10.1002/1521-3773\(20020617\)41:12<2034::AID-ANIE2034>3.0.CO;2-M](https://doi.org/10.1002/1521-3773(20020617)41:12<2034::AID-ANIE2034>3.0.CO;2-M).
- [4] W.M. Huang, B. Yang, Y. Zhao, and Z. Ding, "Thermo-moisture responsive polyurethane shape-memory polymer and composites: A review," *J. Mater. Chem.*, vol. 20, no. 17, pp. 3367–3381, 2010, doi: [10.1039/b922943d](https://doi.org/10.1039/b922943d).
- [5] P. Mora, C. Jubsilp, C.H. Ahn, and S. Rimdusit, "Two-way thermo-responsive thermoset shape memory polymer based on benzoxazine/urethane alloys using as self-folding structures," *Adv. Ind. Eng. Polym. Res.*, vol. 6, no. 1, pp. 13–23, 2023, doi: [10.1016/j.aiepr.2022.09.001](https://doi.org/10.1016/j.aiepr.2022.09.001).
- [6] A. Pandey, G. Singh, S. Singh, K. Jha, and C. Prakash, "3D printed biodegradable functional temperature-stimuli shape memory polymer for customized scaffoldings," *J. Mech. Behav. Biomed. Mater.*, vol. 108, p. 103781, 2020, doi: [10.1016/j.jmbbm.2020.103781](https://doi.org/10.1016/j.jmbbm.2020.103781).
- [7] M. Nabavian Kalat *et al.*, "Investigating a shape memory epoxy resin and its application to engineering shape-morphing devices empowered through kinematic chains and compliant joints," *Mater. Des.*, vol. 233, p. 112263, 2023, doi: [10.1016/j.matdes.2023.112263](https://doi.org/10.1016/j.matdes.2023.112263).
- [8] A. Lendlein, H. Jiang, O. Jünger, and R. Langer, "Light-induced shape-memory polymers," *Nature*, vol. 434, no. 7035, pp. 879–882, 2005, doi: [10.1038/nature03496](https://doi.org/10.1038/nature03496).
- [9] W. Prasomsin, T. Parnklang, C. Sapcharoenkun, S. Tiptipakorn, and S. Rimdusit, "Multiwalled carbon nanotube reinforced bio-based benzoxazine/epoxy composites with NIR-laser stimulated shape memory effects," *Nanomaterials*, vol. 9, no. 6, p. 881, 2019, doi: [10.3390/nano9060881](https://doi.org/10.3390/nano9060881).
- [10] B. Yang, W.M. Huang, C. Li, C.M. Lee, and L. Li, "On the effects of moisture in a polyurethane shape memory polymer," *Smart Mater. Struct.*, vol. 13, no. 1, pp. 191–195, 2004, doi: [10.1088/0964-1726/13/1/022](https://doi.org/10.1088/0964-1726/13/1/022).
- [11] Q. Ze *et al.*, "Magnetic Shape Memory Polymers with Integrated Multifunctional Shape Manipulation," *Adv. Mater.*, vol. 32, no. 4, p. 1906657, 2020, doi: [10.1002/adma.201906657](https://doi.org/10.1002/adma.201906657).
- [12] H. Tobushi, R. Matsui, K. Takeda, and E.A. Pieczyska, *Mechanical Properties of Shape Memory Materials*. New York: Nova Science Publishers, 2013.
- [13] W.M. Huang, B. Yang, and Y.Q. Fu, *Polyurethane Shape Memory Polymers*. Boca Raton: CRC Press, Taylor & Francis, 2012.
- [14] C. Liu, H. Qin, and P. T. Mather, "Review of progress in shape-memory polymers," *J. Mater. Chem.*, vol. 17, no. 16, pp. 1543–1558, 2007, doi: [10.1039/b615954k](https://doi.org/10.1039/b615954k).
- [15] K. Strzelec, N. Sienkiewicz, and T. Szmeczyk, "Classification of Shape-Memory Polymers, Polymer Blends, and Composites," in *Shape Memory Polymers, Blends and Composites: Advances and Applications*. J. Parameswaranpillai, S. Siengchin, J.J. George, and S. Jose, Eds. Singapore: Springer Singapore, 2020, pp. 21–52, doi: [10.1007/978-981-13-8574-2](https://doi.org/10.1007/978-981-13-8574-2).
- [16] H. Tobushi, T. Hashimoto, N. Ito, S. Hayashi, and E. Yamada, "Shape Fixity and Shape Recovery in a Film of Shape Memory Polymer of Polyurethane Series," *J. Intell. Mater. Syst. Struct.*, vol. 9, no. 2, pp. 127–136, 1998, doi: [10.1177/1045389X9800900206](https://doi.org/10.1177/1045389X9800900206).
- [17] M. Staszczak *et al.*, "Characterization of Polyurethane Shape Memory Polymer and Determination of Shape Fixity and Shape Recovery in Subsequent Thermomechanical Cycles," *Polymers*, vol. 14, no. 21, p. 4775, 2022, doi: [10.3390/polym14214775](https://doi.org/10.3390/polym14214775).

- [18] M. Bil, M. Jurczyk-Kowalska, K. Kopeć, and M. Heljak, "Study of Correlation between Structure and Shape-Memory Effect/Drug-Release Profile of Polyurethane/Hydroxyapatite Composites for Antibacterial Implants," *Polymers*, vol. 15, no. 4, p. 938, 2023, doi: [10.3390/polym15040938](https://doi.org/10.3390/polym15040938).
- [19] S. Jape *et al.*, "Self-foldable origami reflector antenna enabled by shape memory polymer actuation," *Smart Mater. Struct.*, vol. 29, no. 11, p. 115011, 2020, doi: [10.1088/1361-665X/abaac2](https://doi.org/10.1088/1361-665X/abaac2).
- [20] S. K. Melly, L. Liu, Y. Liu, and J. Leng, "Active composites based on shape memory polymers: overview, fabrication methods, applications, and future prospects," *J. Mater. Sci.*, vol. 55, no. 25, pp. 10975–11051, 2020, doi: [10.1007/s10853-020-04761-w](https://doi.org/10.1007/s10853-020-04761-w).
- [21] G. Scalet, "Two-way and multiple-way shape memory polymers for soft robotics: An overview," *Actuators*, vol. 9, no. 1, 2020, doi: [10.3390/act9010010](https://doi.org/10.3390/act9010010).
- [22] N. Ahmed, B. Niaz, S. Ahmed, M.T. Javid, M. Ali, and M. Tariq, "Mechanically robust and highly elastic thermally induced shape memory polyurethane based composites for smart and sustainable robotic applications," *Polym. Adv. Technol.*, vol. 34, no. 4, pp. 1075–1419, 2023, doi: [10.1002/pat.5961](https://doi.org/10.1002/pat.5961).
- [23] J. Hu, H. Meng, G. Li, and S. I. Ibekwe, "A review of stimuli-responsive polymers for smart textile applications," *Smart Mater. Struct.*, vol. 21, no. 5, 2012, doi: [10.1088/0964-1726/21/5/053001](https://doi.org/10.1088/0964-1726/21/5/053001).
- [24] Y. Shi, H. Chen, and X. Guan, "High shape memory properties and high strength of shape memory polyurethane nanofiber-based yarn and coil," *Polym. Test.*, vol. 101, p. 107277, 2021, doi: [10.1016/j.polymertesting.2021.107277](https://doi.org/10.1016/j.polymertesting.2021.107277).
- [25] H. Garg, J. Mohanty, P. Gupta, A. Das, B.P. Tripathi, and B. Kumar, "Effect of heat-set temperature on the crease recovery behavior of cotton fabric dip-coated with shape memory polyurethane," *Mater. Chem. Phys.*, vol. 294, p. 126952, 2023, doi: [10.1016/j.matchemphys.2022.126952](https://doi.org/10.1016/j.matchemphys.2022.126952).
- [26] H. Jia, S.Y. Gu, and K. Chang, "3D printed self-expandable vascular stents from biodegradable shape memory polymer," *Adv. Polym. Technol.*, vol. 37, no. 8, pp. 3222–3228, 2018, doi: [10.1002/adv.22091](https://doi.org/10.1002/adv.22091).
- [27] M. Ramezani and M.B.B. Monroe, "Biostable Segmented Thermoplastic Polyurethane Shape Memory Polymers for Smart Biomedical Applications," *ACS Appl. Polym. Mater.*, vol. 4, no. 3, pp. 1956–1965, 2022, doi: [10.1021/acsapm.1c01808](https://doi.org/10.1021/acsapm.1c01808).
- [28] Y.C. Jung and J.W. Cho, "Application of shape memory polyurethane in orthodontic," *J. Mater. Sci. Mater. Med.*, vol. 21, no. 10, pp. 2881–2886, 2010, doi: [10.1007/s10856-008-3538-7](https://doi.org/10.1007/s10856-008-3538-7).
- [29] A. Bruni, F. G. Serra, A. Deregibus, and T. Castroflorio, "Shape-memory polymers in dentistry: Systematic review and patent landscape report," *Materials*, vol. 12, no. 14, p. 2216, 2019, doi: [10.3390/ma12142216](https://doi.org/10.3390/ma12142216).
- [30] G.I. Taylor and M.A. Quinney, "The latent energy remaining in a metal after cold working," *Proc. R. Soc. Lond. A*, vol. 143, no. 849, pp. 307–326, 1934, doi: [10.1098/rspa.1934.0004](https://doi.org/10.1098/rspa.1934.0004).
- [31] M.B. Bever, D.L. Holt and A.L. Titchener, "The Stored Energy of Cold Work," *Prog. Mater. Sci.*, vol. 17, pp. 5–177, 1973, doi: [10.1016/0079-6425\(73\)90001-7](https://doi.org/10.1016/0079-6425(73)90001-7).
- [32] W.S. Farren and G.I. Taylor, "The heat developed during plastic extension of metals," *Proc. R. Soc. Lond. A*, vol. 107, no. 743, pp. 422–451, 1925, doi: [10.1098/rspa.1925.0034](https://doi.org/10.1098/rspa.1925.0034).
- [33] A. Chrysochoos and G. Martin, "Tensile Test Microcalorimetry for Thermomechanical Behaviour Law Analysis," *Mater. Sci. Eng. A*, vol. 108, pp. 25–32, 1989, doi: [10.1016/0921-5093\(89\)90402-4](https://doi.org/10.1016/0921-5093(89)90402-4).
- [34] A. Chrysochoos, O. Maissonneuve, G. Martin, H. Caumon, and J.C. Chezeaux, "Plastic and dissipated work and stored energy," *Nucl. Eng. Des.*, vol. 114, no. 3, pp. 323–333, 1989, doi: [10.1016/0029-5493\(89\)90110-6](https://doi.org/10.1016/0029-5493(89)90110-6).
- [35] A. Chrysochoos and H. Louche, "An infrared image processing to analyse the calorific effects accompanying strain localization," *Int. J. Eng. Sci.*, vol. 38, no. 16, pp. 1759–1788, 2000, doi: [10.1016/S0020-7225\(00\)00002-1](https://doi.org/10.1016/S0020-7225(00)00002-1).
- [36] J. Hodowany, G. Ravichandran, A.J. Rosakis, and P. Rosakis, "Partition of plastic work into heat and stored energy in metals," *Exp. Mech.*, vol. 40, pp. 113–123, 2000, doi: [10.1007/BF02325036](https://doi.org/10.1007/BF02325036).
- [37] W. Oliferuk, and M. Maj, "Stress–strain curve and stored energy during uniaxial deformation of polycrystals," *Eur. J. Mech. A Solids*, vol. 28, no. 2, pp. 266–272, 2009, doi: [10.1016/j.euromechsol.2008.06.003](https://doi.org/10.1016/j.euromechsol.2008.06.003).
- [38] G.W. Adams and R.J. Farris, "Latent energy of deformation of bisphenol a polycarbonate," *J. Polym. Sci. B*, vol. 26, no. 2, pp. 433–445, 1988, doi: [10.1002/polb.1988.090260216](https://doi.org/10.1002/polb.1988.090260216).
- [39] G.W. Adams and R.J. Farris, "Latent energy of deformation of amorphous polymers: 1. Deformation calorimetry," *Polymer*, vol. 30, no. 10, pp. 1824–1828, 1989, doi: [10.1016/0032-3861\(89\)90352-2](https://doi.org/10.1016/0032-3861(89)90352-2).
- [40] O.B. Salamatina, S.N. Rudnev, V.V. Voennyi, and E.F. Oleynik, "Heat and stored energy of plastic deformation of solid polymers and heterogeneous blends," *J. Therm. Anal.*, vol. 38, pp. 1271–1281, 1992, doi: [10.1007/BF01979186](https://doi.org/10.1007/BF01979186).
- [41] D. Rittel, "An investigation of the heat generated during cyclic loading of two glassy polymers. part i: Experimental," *Mech. Mater.*, vol. 32, no. 3, pp. 131–147, 2000, doi: [10.1016/S0167-6636\(99\)00051-4](https://doi.org/10.1016/S0167-6636(99)00051-4).
- [42] D. Rittel and Y. Rabin, "An investigation of the heat generated during cyclic loading of two glassy polymers. Part ii: Thermal analysis," *Mech. Mater.*, vol. 32, no. 3, pp. 149–159, 2000, doi: [10.1016/S0167-6636\(99\)00052-6](https://doi.org/10.1016/S0167-6636(99)00052-6).
- [43] D. Kong, J. Li, A. Guo, X. Zhang, and X. Xiao, "Self-healing high temperature shape memory polymer," *Eur. Polym. J.*, vol. 120, p. 109279, 2019, doi: [10.1016/j.eurpolymj.2019.109279](https://doi.org/10.1016/j.eurpolymj.2019.109279).
- [44] B. Heuwers, A. Beckel, A. Krieger, F. Katzenberg, and J.C. Tiller, "Shape-Memory Natural Rubber: An Exceptional Material for Strain and Energy Storage," *Macromol. Chem. Phys.*, vol. 214, pp. 912–923, 2013, doi: [10.1002/macp.201200649](https://doi.org/10.1002/macp.201200649).
- [45] J.M. Muracciole, B. Wattrisse, and A. Chrysochoos, "Energy balance of a semicrystalline polymer during local plastic deformation," *Strain*, vol. 44, no. 6, pp. 468–474, 2008, doi: [10.1111/j.1475-1305.2007.00412.x](https://doi.org/10.1111/j.1475-1305.2007.00412.x).
- [46] E.A. Pieczyńska *et al.*, "Thermomechanical properties of polyurethane shape memory polymer – experiment and modelling," *Smart Mater. Struct.*, vol. 24, no. 4, p. 045043, 2015, doi: [10.1088/0964-1726/24/4/045043](https://doi.org/10.1088/0964-1726/24/4/045043).
- [47] E.A. Pieczyńska *et al.*, "Mechanical and IRT Analysis of Shape Memory Polyurethane," *J. Mater. Eng. Perform.*, vol. 23, no. 7, pp. 2553–2560, 2014, doi: [10.1007/s11665-014-0963-2](https://doi.org/10.1007/s11665-014-0963-2).
- [48] M. Merzlyakov, C. Schick, "Step response analysis in DSC — a fast way to generate heat capacity spectra," *Thermochim. Acta*, vol. 380, no. 1, 2001, pp. 5–12, 2001, doi: [10.1016/S0040-6031\(01\)00631-1](https://doi.org/10.1016/S0040-6031(01)00631-1).

- [49] Y.K. Kwon, Androsch, M. Pyda, and B. Wunderlich, “Multi-frequency sawtooth modulation of a power-compensation differential scanning calorimeter,” *Thermochim. Acta*, vol. 367–368, 2001, pp. 203–215, doi: [10.1016/S0040-6031\(00\)00695-X](https://doi.org/10.1016/S0040-6031(00)00695-X).
- [50] W. Szczepiński, *Experimental methods in mechanics of solids*, Warsaw: PWN-Polish Scientific Publishers, Elsevier Science Publishers, 1990.
- [51] W. Oliferuk, “Proces magazynowania energii i jego strukturalny aspekt podczas jednoosiowego rozciągania stali austenitycznej,” Habilitation thesis, IFTR PAS, Warsaw, 1997.
- [52] M. Maj, “Wpływ kierunku wstępnego odkształcenia na proces magazynowania energii w polikryształach,” PhD thesis, Institute of Fundamental Technological Research Polish Academy of Sciences, Warsaw, 2007.
- [53] Staszczak, E.A. Pieczyska, R. Matsui, and K. Takeda, “Estimation of energy storage and dissipation in Shape Memory Polymer during its deformation,” in *Proc. 41st Solid Mechanics Conf.*, 2018, pp. 338–339.
- [54] E. Ayres, R.L. Orefice, and M.I. Yoshida, “Phase morphology of hydrolysable polyurethanes derived from aqueous dispersions,” *Eur. Polym. J.*, vol. 43, no. 8, pp. 3510–3521, 2007, doi: [10.1016/j.eurpolymj.2007.05.014](https://doi.org/10.1016/j.eurpolymj.2007.05.014).
- [55] D. Alhazov, A. Gradys, P. Sajkiewicz, A. Arinstein, and E. Zusman, “Thermo-mechanical behaviour of electrospun thermoplastic polyurethane nanofibers,” *Eur. Polym. J.*, vol. 49, no. 12, pp. 3851–3856, 2013, doi: [10.1016/j.eurpolymj.2013.09.028](https://doi.org/10.1016/j.eurpolymj.2013.09.028).
- [56] L.E. Alexander. *X-ray Diffraction Methods in Polymer Science*, New York: Wiley-Interscience, 1969.
- [57] W. Thomson (Lord Kelvin), “On the thermoelastic and thermomagnetic properties of matter,” *Trans. R. Soc. Edinburgh*, vol. 20, no. 161, pp. 57–77, 1853.
- [58] E.A. Pieczyska *et al.*, “Experimental and numerical investigation of yielding phenomena in a shape memory polymer subjected to cyclic tension at various strain rates,” *Polym. Test.*, vol. 60, pp. 333–342, 2017, doi: [10.1016/j.polymertesting.2017.04.014](https://doi.org/10.1016/j.polymertesting.2017.04.014).
- [59] E.A. Pieczyska *et al.*, “Investigation of thermomechanical couplings, strain localization and shape memory properties in a shape memory polymer subjected to loading at various strain rates,” *Smart Mater. Struct.*, vol. 25, no. 8, p. 085002, 2016, doi: [10.1088/0964-1726/25/8/085002](https://doi.org/10.1088/0964-1726/25/8/085002).
- [60] M. Staszczak, E.A. Pieczyska, M. Maj, D. Kukla, and H. Tobushi, “Infrared thermographic analysis of shape memory polymer during cyclic loading,” *Meas. Sci. Technol.*, vol. 27, no. 12, pp. 124007, 2016, doi: [10.1088/0957-0233/27/12/124007](https://doi.org/10.1088/0957-0233/27/12/124007).
- [61] H.J. Qi, T.D. Nguyen, F. Castro, C.M. Yakacki, and R. Shandas, “Finite deformation thermomechanical behaviour of thermally induced shape memory polymers,” *J. Mech. Phys. Solids*, vol. 56, no. 5, pp. 1730–1751, 2008, doi: [10.1016/j.jmps.2007.12.002](https://doi.org/10.1016/j.jmps.2007.12.002).
- [62] E.A. Pieczyska, S.P. Gadaj, W.K. Nowacki, K. Hoshio, Y. Maki-no, and H. Tobushi, “Characteristics of energy storage and dissipation in TiNi shape memory alloy,” *Sci. Technol. Adv. Mater.*, vol. 6, no.8, pp. 889–894, 2005, doi: [10.1016/j.stam.2005.07.008](https://doi.org/10.1016/j.stam.2005.07.008).